Tip-induced inversion of the chirality of a molecule's adsorption potential probed by the switching directionality

A. Bauer, M. Maier, W. Schosser, J. Diegel, F. Paschke, Y. S. Dedkov, Fabian Pauly, R. Winter, M. Fonin

Angaben zur Veröffentlichung / Publication details:

Bauer, A., M. Maier, W. Schosser, J. Diegel, F. Paschke, Y. S. Dedkov, Fabian Pauly, R. Winter, and M. Fonin. 2020. "Tip-induced inversion of the chirality of a molecule's adsorption potential probed by the switching directionality." *Advanced Materials* 32 (12): 1907390.

ADVANCED MATERIALS
www.advmat.de

Tip-Induced Inversion of the Chirality of a Molecule's Adsorption Potential Probed by the Switching Directionality

*Anja Bauer, Markus Maier, Werner M. Schosser, Josefine Diegel, Fabian Paschke, Yuriy Dedkov, Fabian Pauly, Rainer F. Winter, and Mikhail Fonin**

The switching behavior of surface-supported molecular units excited by current, light, or mechanical forces is determined by the shape of the adsorption potential. The ability to tailor the energy landscape in which a molecule resides at a surface gives the possibility of imposing a desired response, which is of paramount importance for the realization of molecular electronic units. Here, by means of scanning tunneling microscopy, a triazatruxene (TAT) molecule on Ag(111) is studied, which shows a switching behavior characterized by transitions of the molecule between three states, and which is attributed to three energetically degenerate bonding configurations. Upon tunneling current injection, the system can be excited and continuously driven, showing a switching directionality close to 100%. Two surface enantiomers of TAT show opposite switching directions pointing at the chirality of the energy landscape of the adsorption potential as a key ingredient for directional switching. Further, it is shown that by tuning the tunneling parameters, the symmetry of the adsorption potential can be controllably adjusted, leading to a suppression of the directionality or an inversion of the switching direction. The findings represent a molecule-surface model system exhibiting unprecedented control of the shape of its adsorption potential.

The understanding of the switching behavior of molecular systems[1] is of specific importance for the realization of active units in future information processing and storage devices. In particular, switching processes at surfaces have been studied intensely by scanning probe techniques, including investigations of switching based on rotational motion of molecules,[2–7] molecular conformational changes,[8–11] intramolecular hydrogen transfer,[12–20] chemical changes in molecules,[21,22] and charge-state transitions of single molecules.[23] The switching process itself can be driven either by thermal activation[2,4] or by external means, including energy transfer from inelastically scattered electrons[2,12,14–16] or photons,[8,24] as well as the application of mechanical forces.[17,25,26] Independent of how the switching is activated, the switching behavior is defined by the landscape of the energy potential. Its controlled and precise manipulation will ensure the possibility of tuning the number of accessible states and switching rates, allowing the system to be reliably programmed.

In this work, we investigate triazatruxene (TAT) molecules on a Ag(111) surface deposited by the electrospray method.[27,28] **Figure 1**a shows a large-scale scanning tunneling microscopy (STM) image of individual TAT molecules on Ag(111). The observed intramolecular contrast suggests the presence of several adsorption configurations, which will be discussed in the following. Figure 1b shows a typical high-resolution STM image of a TAT molecule. Its trigonal symmetry is marked by three main maxima (see line profiles in Figure 1c), two of which are accompanied by half-circle-shaped depressions on the metal substrate. Between the main maxima a boomerang-shaped feature together with a less pronounced round protrusion are visible. The comparison with the adsorption geometries calculated by density functional theory (DFT) and their energies suggests that the TAT molecules adsorb on atop sites (Figure 1d,e), i.e., the central benzene ring of TAT is placed above a silver (Ag) atom, with the three nitrogen (N) atoms of the corresponding pyrrole units also located above Ag atoms. The ethyl groups attached to the N atoms point away from the substrate, yielding the three main maxima observed by STM (Figure 1b), while features in between the maxima can be attributed to the molecular backbone. For the optimized

A. Bauer, W. M. Schosser, J. Diegel, F. Paschke, Prof. F. Pauly, Prof. M. Fonin
Fachbereich Physik
Universität Konstanz
78457 Konstanz, Germany
E-mail: mikhail.fonin@uni-konstanz.de

M. Maier, Prof. R. F. Winter
Fachbereich Chemie
Universität Konstanz
78457 Konstanz, Germany

W. M. Schosser, Prof. F. Pauly
Okinawa Institute of Science and Technology Graduate University
Onna-son
Okinawa 904-0495, Japan

Prof. Y. Dedkov
Department of Physics
Shanghai University
99 Shangda Road, 200444 Shanghai, China

The ORCID identification number(s) for the author(s) of this article can be found under https://doi.org/10.1002/adma.201907390.

DOI: 10.1002/adma.201907390

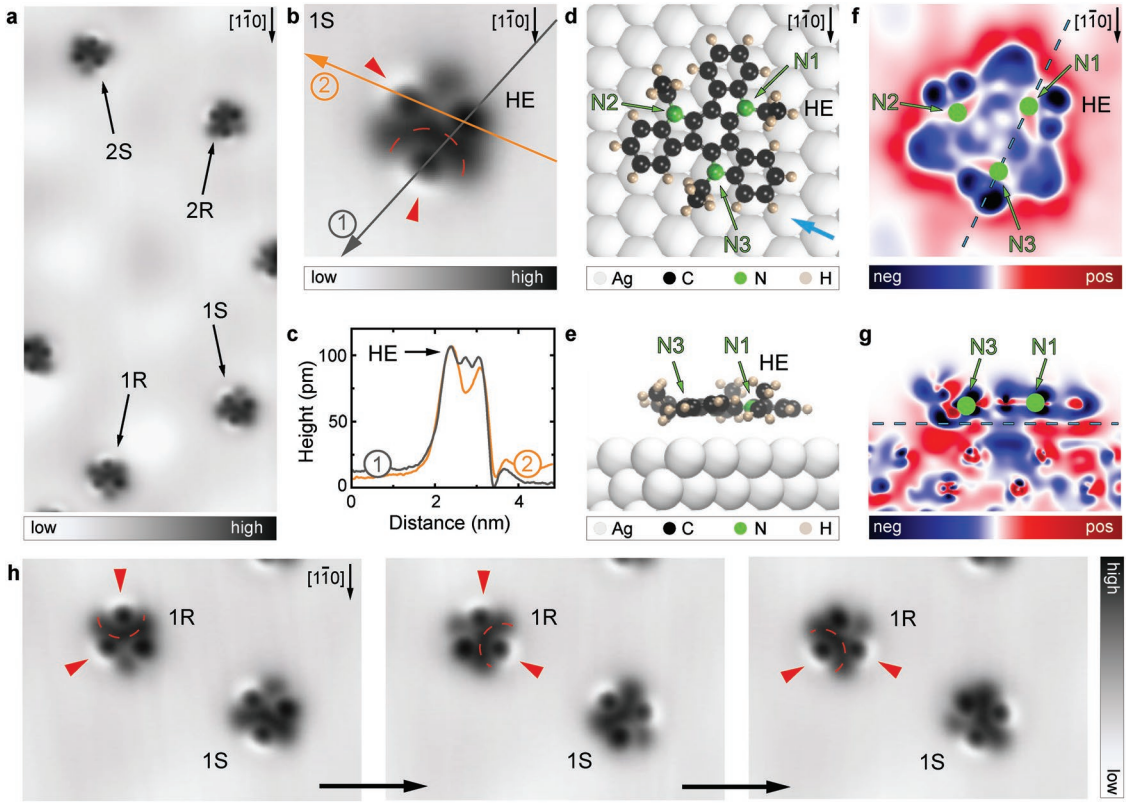

Figure 1. TAT molecules on Ag(111). a) Large-scale STM image of TAT molecules on Ag(111) (U = 10 mV, I = 100 pA, 9 × 18 nm^2). b) STM image of a single TAT molecule (1S-type) (U = 10 mV, I = 100 pA, 3 × 3 nm^2). The highest ethyl group is marked as HE. Depressions localized close to the other ethyl groups are denoted by red triangles and the boomerang-shaped feature within the molecule by a dashed red semicircle. c) Height profiles along the gray and orange lines shown in (b). d) Optimized adsorption geometry of TAT on Ag(111) (1S-type). The theoretical studies suggest that TAT molecules adsorb on atop sites, meaning that the central benzene ring is located above a Ag atom. This can be further specified into atop-fcc (pyrrole above fcc-hollow sites) and atop-hcp adsorption sites (pyrrole above hcp-hollow sites), referred to as 1 and 2. Additionally, the presence of the surface leads to two non-superimposable configurations of the TAT molecule labeled as R and S. Four possible adsorption types—1R, 1S, 2R, and 2S—are indicated by arrows in (a). e) Side view of the DFT-optimized adsorption geometry along the view direction marked by a blue arrow in (d). f,g) Charge-density difference calculated as $\Delta\rho(\mathbf{r}) = \rho_{TAT/Ag}(\mathbf{r}) - \rho_{Ag}(\mathbf{r}) - \rho_{TAT}(\mathbf{r})$ and plotted in units of e nm^{-3} for geometry (d) and (e), respectively. Signs are chosen such that a positive charge or missing electrons are counted as positive. The color scale ranges from –4 e nm^{-3} (blue) to 4 e nm^{-3} (red), where e = |e| is the elementary charge. Cut plane positions are marked by blue dashed lines in (f) and (g). h) A series of subsequently recorded STM images of two TAT molecules showing switching between three equivalent bonding configurations within their adsorption types—1R and 1S (U = 10 mV, I = 100 pA, 7 × 5 nm^2). Characteristic molecular features are highlighted by red triangles and dashed red semicircles.

geometry, the dispersion-corrected DFT calculations predict a binding energy of $E_B = -E_{TAT/Ag} + E_{TAT} + E_{Ag}$ = 1.053 eV per molecule. By analyzing the charge transfer at the molecule–metal interface (see Figure 1f,g), we conclude that the binding is not only due to purely nonlocal van der Waals (vdW) interaction, but shows contributions from electrostatic interaction. In the areas of the substrate, where N atoms are located above Ag atoms, the charge density difference is positive (Figure 1f,g). Moreover, a strong charge redistribution is observed for the methylene moiety of the ethyl group attached to the nitrogen with the C atom coming close to the Ag(111) surface. As a result, the corresponding C—N bond is almost parallel to the surface plane. The molecule is thus effectively pinned at three nitrogen-related anchoring points. The DFT calculations reveal that the three N—Ag bonds are not equivalent, showing different vertical distances of N atoms to the Ag surface plane: z_{N1} = 3.64 Å, z_{N2} = 3.62 Å, and z_{N3} = 3.61 Å. The same trend is observed for the C atoms of the methylene groups, which come even closer to the Ag surface. Thus, for the two anchoring points with a shorter z-distance to the Ag surface a stronger interaction is expected. This is accompanied by a larger charge redistribution with positive charge accumulation in the surface plane in close proximity to the methylene groups, which results in two electron depletion areas in the substrate, imaged by STM as depressions[29] (marked by red triangles in Figure 1b). The vertical distance of N1 is slightly longer than of N2 and N3, showing less charge redistribution and no depletion area around the corresponding methylene group. This results in a slight tilt of the whole molecule with the corresponding ethyl group being pushed away from the surface plane (marked as highest ethyl (HE) in Figure 1c). We note that the observed charge redistribution at the interface gives rise to the formation of a surface dipole, which induces a repulsive interaction[30] between neighboring TAT molecules. For low coverages, this leads to the formation of quasiperiodic arrays with large intermolecular distances (Figure 1a).

Taking into account the threefold symmetry of the molecule, one can expect three bonding configurations within the same adsorption geometry, depending on which of the N and C atoms are furthest to the underlying Ag plane at the anchoring points. In STM images, the three configurations are clearly distinguishable by the positions of the depletion areas (Figure 1h). High-resolution images show that two orientations of TAT exist owing to two possible adsorption sites: atop-fcc and atop-hcp, meaning that the central carbon ring of TAT is located above a Ag atom and the neighboring pyrrole rings are located either above face-centered-cubic (fcc) or hexagonal-close-packed (hcp) hollow sites. These configurations are denoted as 1 and 2 in the following. Additionally, we find that two non-superimposable configurations of the TAT molecule emerge upon adsorption due to the surface-binding of a prochiral TAT molecule via either its Re or Si face, which are labeled as R and S (Figure 1a). Right- and left-handed molecules can be distinguished by the position of the depletion areas with respect to the boomerang-shaped intensity within the molecule's interior. Thus, two adsorption sites together with two chiral forms for each adsorption site (1R, 1S and 2R, 2S), as well as three bonding configurations for each of the four adsorption types result in a total of twelve different states, which can be unambiguously assigned in STM images (Figure 1h and Figure 3a later).

We observe that, upon scanning, TAT molecules switch between the three bonding configurations defined by the different z-distances of the N atoms to the Ag plane at the three anchoring points. A sequence of STM images presented in Figure 1h illustrates the switching process of two TAT molecules (1R and 1S). In particular, the position of the depletion areas and of the boomerang-shaped feature inside the molecule with respect to the surface crystallographic axes is indicative for each of the states. We suggest the switching to occur by a simultaneous interchange of the bond lengths and thus the z-distances of the N and C atoms to the Ag plane for all three anchoring sites, leading to a redistribution of the electron density, and finally to changes in the local tunneling conductance. Thus, we reveal a novel realization of an on-surface molecular switch based on the jiggling between three degenerate surface bonding configurations within the same adsorption site. To support the proposed switching mechanism, we discuss further possible scenarios. A switching by rotation[2–7] can be excluded, as TAT/Ag(111) does not possess a rotational axis and shows the same switching behavior in dense layers (Figure S1, Supporting Information). Another possibility is conformational switching,[11] involving the conformational motion of the ethyl groups. However, this scenario is improbable, since the ethyl groups are constrained by the strong interaction with the Ag(111) surface. Moreover, conformational changes of individual ethyl groups would result in a larger number of distinct molecular states, which we do not observe in our experiments. Nevertheless, the ethyl groups play a crucial role in the bonding and their precise configuration is essential for the description of the molecules' adsorption geometry.

We focus now on the dynamics of the observed switching at different scanning parameters. Increasing the tunneling current or the bias voltage leads to a strong increase of the switching rate. This does not allow imaging of the states separately but only of their superposition, resulting in a symmetrical appearance of the TAT molecule (**Figure 2**a). However, the fast switching process causes fluctuations of the tunneling current, whose spatial distribution can be detected in the STM topography. Figure 2b shows the simultaneously recorded tunneling current image, which reveals that three main noise clouds represented by huge current fluctuations are localized close to the ethyl groups. The chosen color scale highlights the current fluctuations around I_{set} = 500 pA and suppresses the molecular contrast. The three main clouds constitute a propeller-like noise feature, which reflects the molecule's chirality. We note that the clouds spread into the Ag surface, meaning that the switching can also be induced aside of the molecule. This can be possibly facilitated by excitation of surface plasmons[31] or by hot electrons.[20] We investigated the switching behavior in detail by positioning the tip above a TAT molecule and recording the time evolution of the z-position of the STM tip at different points (Figure 2a,b). During the measurements the feedback remained turned on with the tip regulation time chosen in a way to minimize the effect on the measurement. All presented time traces $z(t)$ are background-corrected by subtracting the slow z-variations due to temperature drift from the measurement signal, thus yielding the time-dependent variation of the relative z-position Δz. We also performed exemplary $I(t)$ measurements in parallel to $z(t)$ with no deviations in switching behavior being observed. Figure 2c (upper panel) presents the time dependence of the relative z-position of the scanner, revealing a telegraph noise signal with well-separated high-z (HZ), middle-z (MZ), and low-z (LZ) states. The residence times as well as the separation between the states were found to strongly depend on the exact tip position (see Figure S2 in the Supporting Information). Here, we concentrate on points, where the tip is positioned within a noise cloud either above the molecule (point 1) or above the Ag substrate aside of the molecule (point 2). The former is characterized by the three-state telegraph noise with almost equally separated states and comparable switching rates for all transitions. Shifting the tip position away from the molecule leads to a strong change of the relative height of the MZ state. Now, the MZ state overlaps with the LZ state, which overall results in an almost perfect two-state (HZ↔LZ/MZ) telegraph noise characteristic (Figure 2c, lower panel). We attribute this behavior to the conductance difference between the areas with or without an electrostatic depletion.

Figure 2d shows the voltage dependence of the switching rate in the range of ±100 mV recorded at point 1. For the voltage range of low switching rates (0–45 meV) measurements over several hours were performed yielding at least 35 events for each point. For the range 50–65 meV 100–600 events per point were evaluated. For high switching rates above 65 meV we considered 600–7500 events per point. No data could be recorded for fast switching rates at bias voltages exceeding ±100 mV and I_{set} = 500 pA, as the measurements are limited by the time resolution of the STM electronics. For bias voltage values between 0 and ±40 mV a very low constant switching rate is observed. For the absolute values exceeding 40 mV, we observe a rapid increase of the switching rate by about five orders of magnitude. Switching rates at negative bias voltages behave similarly to positive ones, resulting in a symmetric behavior around the

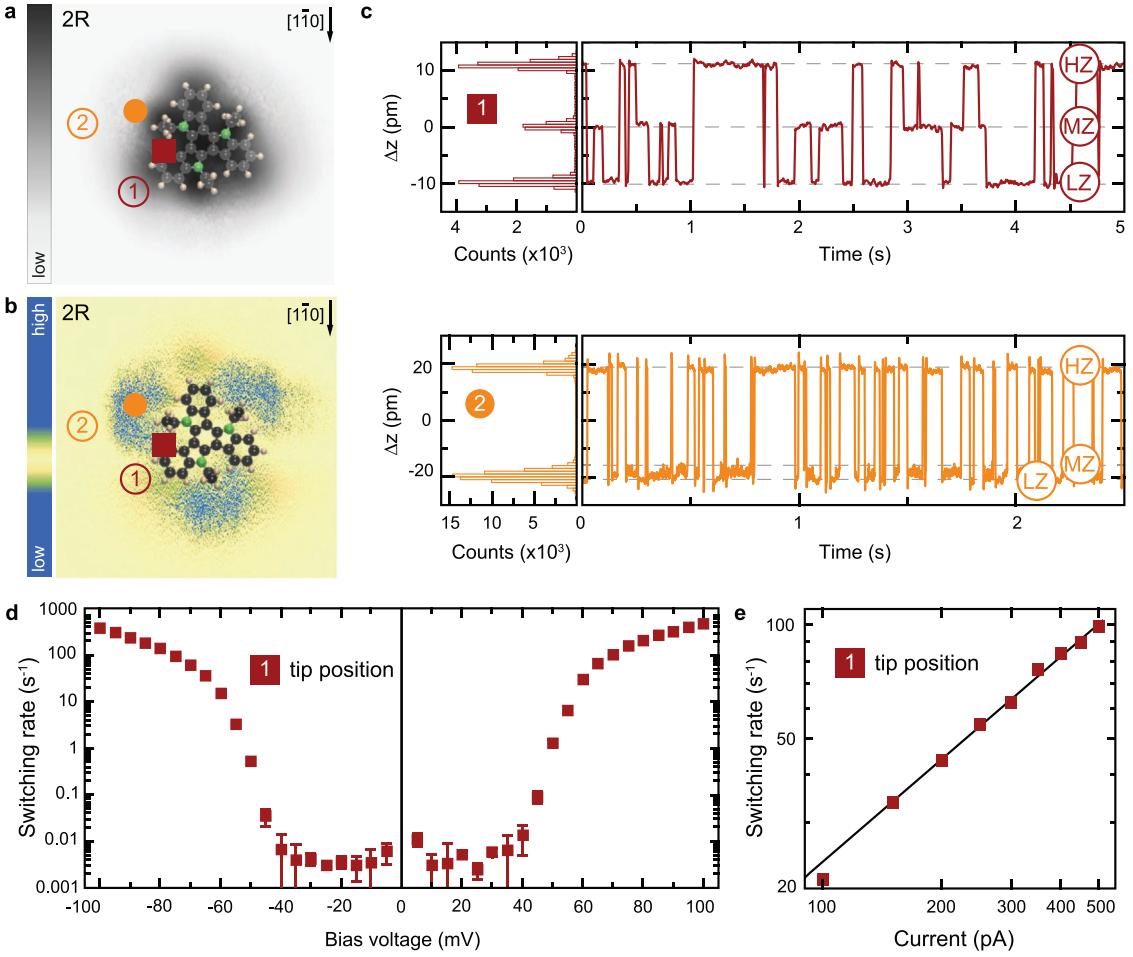

Figure 2. Current-induced switching of single TAT molecules. a) STM image of a single TAT molecule (2R-type) recorded at a bias voltage of 200 mV (I = 500 pA, 3 × 3 nm^2) with the corresponding molecular structure superimposed to scale. The color scale ranges from 0 to 100 Å. b) Simultaneously recorded tunneling current image showing conductance fluctuations around I = 500 pA due to switching. The color scale ranges from 320 to 745 pA, with bright yellow corresponding to I = 500 pA and saturated blue-colored regions representing the current values below 450 pA and above 550 pA. c) Time dependencies of the relative tip height Δz (drift corrected) with the corresponding distribution histograms for the two measurement points marked in (a) and (b) (U = 80 mV, I_{set} = 100 pA). A switching between three height values that represent three bonding configurations is clearly visible. d) Bias dependence of the switching rate $r(U)$ measured at position 1. A similar behavior for both polarities is observed, which is characterized by a steep increase starting at about 40 mV (I_{set} = 500 pA). e) Dependence of the switching rate $r(I)$ on the tunneling current recorded at position 1 (U_{set} = 70 mV).

Fermi energy (Figure 2d and Figure S3, Supporting Information). This corroborates that inelastic electron scattering triggers the switching process. Figure 2e shows the analysis of the switching rate as a function of the tunneling current for point 1. The power law fit $r(I) \propto I^n$, yields an exponent of $n = 0.90 \pm 0.03$, indicating that a single-electron process triggers the switching.[14] This behavior in combination with the voltage-dependent data suggests that the switching involves the excitation of a vibrational jiggling mode of the molecule on the surface at about 40 meV by the tunneling electrons. The possibility of a molecular-orbital-supported electron transfer process can be excluded, because tunneling spectra recorded in the vicinity of the Fermi level are rather flat and featureless (Figure S4, Supporting Information). The spectroscopic measurements are consistent with DFT calculations of the ionization potential and the electron affinity of a TAT molecule in the gas phase, yielding an electronic quasiparticle gap of around 6 eV. Thus, we suggest that for higher bias voltages the switching involves vibrational excitations at the molecule–metal interface.

The overall switching behavior (switching rates and dwell times) of the molecule can be effectively manipulated by the vertical tip–sample distance (tunneling current) as well as the lateral tip position above the molecule. For point 1 (see Figure 2c) we observe comparable switching rates for all transitions, which points at similar potential barriers. Analyzing the dwell times for the three states as a function of bias voltage and tunneling current (Figure S5, Supporting Information), we observe a slight difference in populations for 100 pA with the longest dwell time for LZ. No particular trend is observed for bias voltage variation. Upon changing the tunneling current to 500 pA, we find a particularly long dwell time for LZ, which points at a deeper potential well for it. Moving the tip to point 2 (see Figure 2c), yields a high switching rate between LZ and

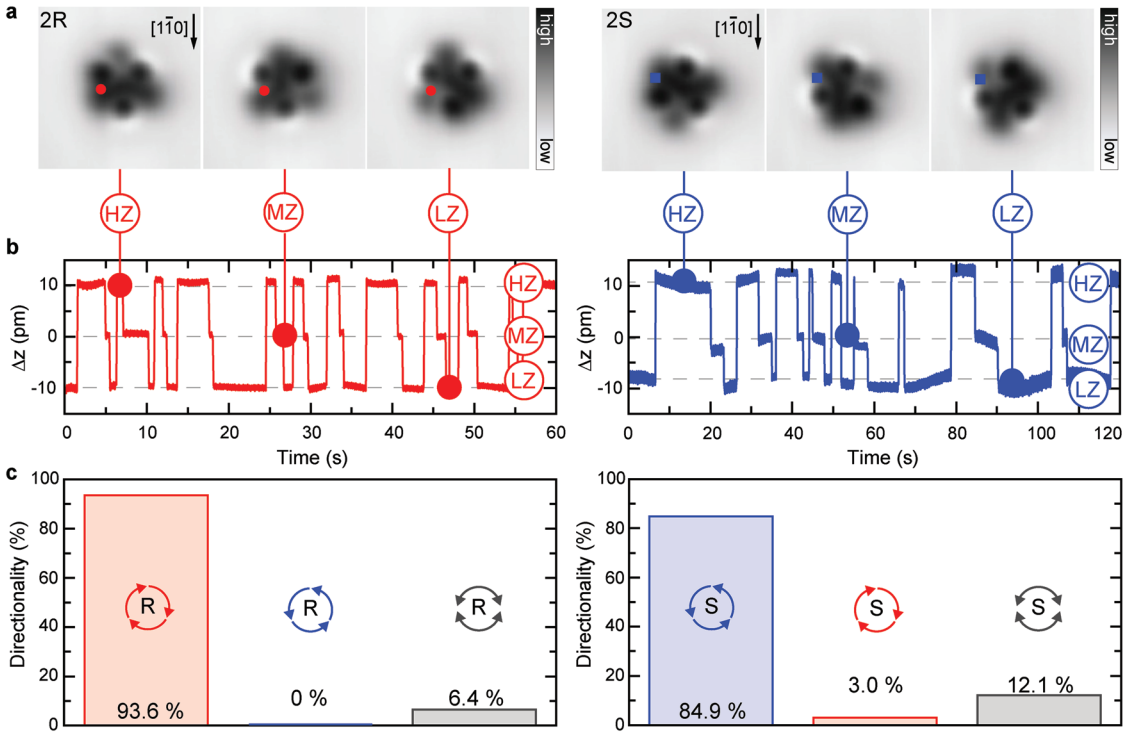

Figure 3. Switching directionality of TAT. a) STM images of the three states involved in the switching for both enantiomers (3×3 nm^2, $U = 10$ mV, $I = 100$ pA). The color scale ranges from 0 to 105 Å. b) Time dependence of the relative height Δz of the tip recorded at 60 mV for the spatial positions marked in (a) ($I_{set} = 100$ pA). For the R-type we observe a clockwise switching (red), whereas the S-type switches anticlockwise (blue), which can be inferred from the positions of the depletion areas and the boomerang-shaped feature on the molecule. c) Histograms showing the distributions of the two-step switching sequences for the two enantiomers of TAT on Ag(111) in the z-time traces presented in (b), respectively. Both show a pronounced switching directionality with the two-step switching sequences {HZ–MZ–LZ}, {MZ–LZ–HZ}, and {LZ–HZ–MZ} reaching together up to 93.6% for the 2R-type and 84.9% for the 2S-type of all possible two-step sequential switching events.

MZ compared to a rather low switching rate toward HZ. This means that the potential barrier toward HZ has become higher, which is an indication of an effective modification of the potential landscape by the tip. Consequently, both vertical and lateral displacements of the STM tip leads to changes in tip-molecule interaction and modification of the potential energy landscape, providing an efficient way to controllably tune the switching behavior.

Let us now study the switching directionality. **Figure 3**a shows the spatially resolved configurations for the three switching states of each enantiomer. The time traces of the z-signal recorded at comparable lateral positions are shown in Figure 3b. From the STM images, HZ, MZ, and LZ can be identified for the chosen tip position above the molecule (marked in Figure 3a). The measurements reveal that the switching process is by no means random, but exhibits a high switching preference, i.e., the repetition of the same sequence of states. For example the system being initially in LZ goes to HZ, then to MZ and ends up in LZ again. This switching sequence is then repeated, meaning that the system is efficiently driven in a given switching direction, as can be deduced from the STM images. For the R-type enantiomer the switching proceeds clockwise (red), whereas it is anticlockwise (blue) for the S-type one. This is evident from the changes in the positions of the depletion areas and the boomerang-shaped feature on the molecule shown in Figure 3a.

In order to obtain reliable statistics of the switching directionality, we recorded multiple time traces of the relative z-position on one of the lateral points of the molecule with fixed tunneling parameters. Further, we analyzed the obtained data in terms of the switching directionality. For this purpose we define a two-step switching sequence as an entity consisting of three successive states related by two transition steps in between these states. Based on this, we studied all two-step switching sequences within each measurement of the z-time trace to obtain the corresponding probability histograms plotted in Figure 3c. In this procedure we consider 12 realizations for two-step switching sequences in the three-level system, which allows the switching preference of the system to be fully characterized (see Figure S6 in the Supporting Information for details). For example, starting initially in the LZ state the system can transition into the MZ state and further to LZ or HZ, alternatively it can go to HZ and then to MZ or LZ. The overall 6 two-step switching sequences including only two states, like {LZ–MZ–LZ} or {LZ–HZ–LZ}, imply that the molecule jumps back and forth between two states, without any directionality. On the other hand the two-step switching sequences including three states like {HZ–MZ–LZ} correspond to a directional switching. Since switching sequences like {HZ–MZ–LZ}, {MZ–LZ–HZ}, and {LZ–HZ–MZ} are permutations and thus all describe the same switching direction, they are added together, yielding a measure for the switching directionality $P = (N_{\{HZ–MZ–LZ\}} + N_{\{MZ–LZ–HZ\}} + N_{\{LZ–HZ–MZ\}})/N_{\Sigma}$, where N_{Σ}

represents the total number of evaluated two-step switching sequences. We discover an exceptionally high directionality for both enantiomers with P_S = 84.9% and P_R = 93.6% (Figure 3). Within our measurements we observed that the directionality shows only little dependence on the tip state, indicating that the molecule–surface interaction, i.e., the chirality of the adsorption potential, is the most important factor responsible for the directional switching.

The theoretical description of the observed directional switching of TAT is a rather complicated task, as a three-dimensional motion of the molecule on the surface has to be considered. Thus, we give a simplified explanation relying on the Brownian ratchet theory.[20,32–34] We consider a motion in a 1D sawtooth potential, whose shape is imposed by the molecule's chirality upon adsorption as shown in **Figure 4**a (left). Due to inelastic electron tunneling, energy can be

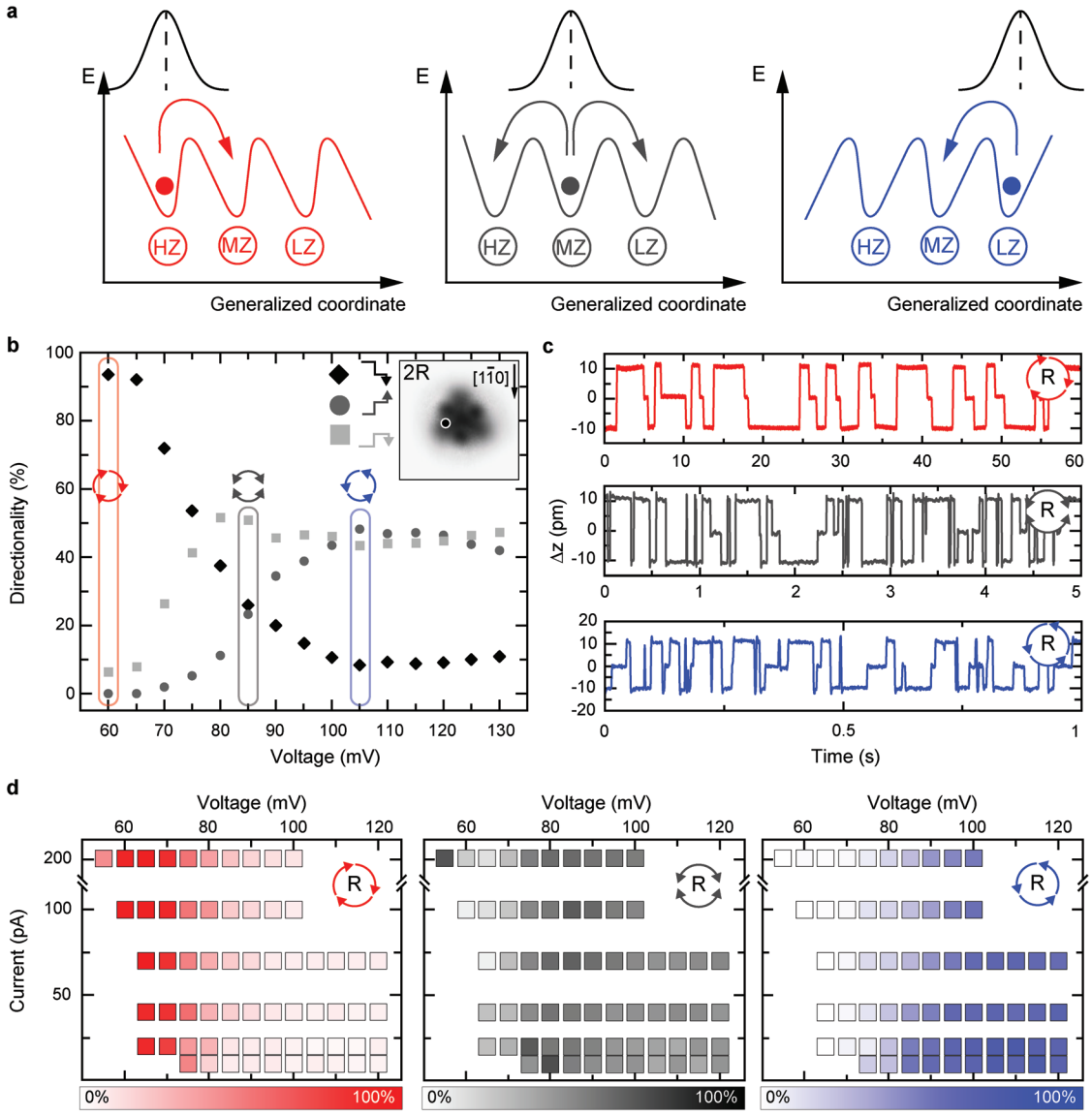

Figure 4. Control of the switching directionality. a) Sketches of generic one-dimensional landscapes of the energy potential with three degenerate states: (left) an asymmetric potential with a steep left slope, (middle) a symmetric one, and (right) an asymmetric one with a steep right slope. The random Gaussian velocity distribution for a particle position at the minimum of the potential is also shown. Within the asymmetric potential landscapes the switching shows high directionality while it is nondirectional for the symmetric one. b) Bias-voltage dependence of the switching directionality of a TAT molecule (2R-type) measured at 100 pA. The measurement position is marked in the inset of (b). The percentage contribution of {HZ–MZ–LZ} two-step sequences is represented by black diamonds, that of {LZ–MZ–HZ} two-step sequences by dark gray circles and that of nondirectional ones by light gray squares. At low bias voltages an exceptionally high degree of directionality is observed, reaching about 94% (clockwise). Upon increasing the voltage the switching behavior changes from clockwise to preferentially anticlockwise (P_{acw} = 50%, P_{cw} = 8%). c) Characteristic time traces of Δz recorded at 60 mV (clockwise), 85 mV (nondirectional), and 105 mV (anticlockwise) for the 2R-type molecule in (b). For all measurements: I_{set}=100 pA. d) Dependence of the directionality on the bias voltage and current for the 2R-type molecule at the same spatial charge-injection point, marked in the inset of (b). Independent of the applied tunneling current, the switching changes with increasing bias voltage from preferentially clockwise to non-directional and then to anticlockwise. The switching goes from 94% clockwise (red, I_{set} = 100 pA, U = 60 mV) to 67% anticlockwise (blue, I_{set} = 20 pA, U = 110 mV), depending on the selected tunneling parameters. The directionality is color-coded (red: clockwise, gray: nondirectional, blue: anticlockwise).

deposited on the molecule, which is transformed into molecular vibration and corresponds to a temperature rise in the ratchet theory. The populated excited state is then relaxing into the ground state inducing a random walk motion. According to Maxwell–Boltzmann statistics, we assume the velocity distribution after the excitation to be Gaussian. The subsequent relaxation process leads to a directed motion, if the potential is spatially asymmetric, as sketched in Figure 4a. Given the very high directionality of the switching process, we believe the potential, which the TAT molecule experiences, to be highly asymmetric with one side being steeper than the other. For both enantiomers we thus observe the same behavior, which however differs by the switching direction due to the different chirality of the adsorption potential.

We systematically studied the switching directionality as a function of tunneling parameters focusing on the R-enantiomer. For our measurements we chose a lateral point, which initially shows a pronounced 3-step switching with almost 100% directionality (clockwise) at I_{set} = 100 pA, U = 60 mV. Figure 4b displays the bias-voltage dependence of the switching directionality. Further measurements for the negative bias voltage range as well as an additional data set, obtained at a tunneling current of I_{set} = 10 pA are presented in Figures S7 and S8 (Supporting Information). The number of events considered is comparable to the statistics used in Figure 2. Furthermore, the analysis of the switching behavior of several tens of single TAT molecules corroborates the results. Typical time traces illustrating the changes in the switching behavior are shown in Figure 4c. We observe a pronounced dependence of the switching behavior on the applied voltage. The effective adsorption potential of TAT on Ag(111) is schematically represented in Figure 4a. Upon variation of the electric field the shape of the potential energy surface is modified going from the asymmetric one (left-hand panel), which favors the clockwise switching, to the symmetric one (middle panel) and further to the asymmetric one (right-hand panel), which favors the anticlockwise switching. This means that the chirality of the potential is effectively inverted and consequently the switching direction as well. This very behavior is observed in the measured bias-voltage dependence, presented in Figure 4b. Increasing the bias voltage from 60 to 85 mV yields a transition from highly directional to nondirectional switching. Going further to 105 mV restores the directionality with inverted switching direction. The effective change of the potential's shape by the variation of the electric field is most probably related to the presence of the surface-dipole moment at the molecule due to adsorption. Consequently, the external field imposed by the STM tip will have a considerable effect on the dipole and will therefore significantly modify the landscape of the potential, resulting in the modified switching behavior, visible in the experiment. The switching directionality can thus be tuned precisely by using appropriate bias-voltage settings. If both current and bias voltage are varied at the same charge-injection point, we detect an even stronger impact on the switching behavior. Figure 4d shows the switching directionality as a function of both, bias voltage and tunneling current, measured at a fixed point above a 2R-type molecule. The effect of the tunneling current is such that the directionality for the anticlockwise switching decreases from around 65% to 50% (blue), when going from I_{set} = 10 to 100 pA for the bias voltage range of U = 100–110 mV. This effect of current is likely related to the distortion of the adsorption potential by the presence of the STM tip, which comes closer to the molecule at higher tunneling currents. The shape of the potential is also modified due to the van der Waals interaction between the tip and the sample at reduced distances. Both effects might lead to a smoothing of the potential landscape, thus lifting the directional switching.

In summary, we have demonstrated that the chiral adsorption potential induced by the presence of a TAT molecule on a Ag(111) surface can be precisely adjusted by appropriate settings of the STM tip in the proximity of the molecule, even allowing the chirality of the energy landscape to be inverted. We were able to show that switching with a directionality close to 100% can be realized. Furthermore, we presented the possibility of suppressing the directionality and restoring it again with the opposite switching direction by decreasing the tip–molecule distance at the same lateral position. Our findings are an important step toward the realization of functional molecular systems with potential applications in the field of nanoscale molecular switching.

Experimental Section

TAT was synthesized following a previously reported procedure.[35] The purity of the final material was verified by nuclear magnetic resonance spectroscopy and mass spectrometry. The clean Ag(111) single crystal (Surface Preparation Laboratory) surface was prepared by repeated cycles of Ar^+ sputtering and subsequent annealing to about 890 K. Electrospray deposition of TAT molecules on the clean Ag(111) surface was performed as described elsewhere.[27,28] The sample was kept at room temperature during deposition, and then transferred into the cryogenic STM (Omicron Nanotechnology GmbH) operated at temperatures of 5–6 K. STM measurements were carried out in the constant-current mode using grinded and polished PtIr tips (Nanoscore GmbH). The sign of the bias voltage corresponds to the potential at the sample.

Theoretical DFT calculations were performed using the quantum chemistry code TURBOMOLE (version 7.1),[36] employing the def-SV(P) Gaussian basis set[37] and the Perdew–Burke–Ernzerhof (PBE) exchange-correlation functional.[38] In order to take van der Waals interactions into account, a dispersion correction to the PBE functional was employed.[39] Total energies were converged to a precision of better than 10^{-6} a.u., and geometry optimizations were carried out until the change of the maximum norm of the Cartesian gradient was below 10^{-5} a.u. A slab of three Ag layers was used as the substrate, in which the positions of the atoms in the upper two metal layers below the molecule were allowed to relax, while the bottom layer was held fixed at bulk lattice values.

Supporting Information

Supporting Information is available from the Wiley Online Library or from the author.

Acknowledgements

This work was financially supported by the Deutsche Forschungsgemeinschaft (DFG) through SFB 767 "Controlled Nanosystems" and through FO 640/7-1.

Conflict of Interest

The authors declare no conflict of interest.

Author Contributions

M.F. conceived of the experiments. A.B., J.D., F.Paschke, Y.D., and M.F. performed the experiments. A.B. and M.F. analyzed the data and drafted the manuscript. M.M. and R.F.W. performed the chemical synthesis. W.M.S. and F.Pauly performed the DFT calculations. All authors discussed the results and contributed to writing the paper.

Keywords

molecular electronics, molecular switches, molecules on surfaces, molecular charge states, scanning tunneling microscopy

Received: November 11, 2019
Revised: December 27, 2019
Published online: February 17, 2020

[1] B. L. Feringa, W. R. Browne, *Molecular Switches*, Wiley-VCH, Weinheim, Germany **2011**.
[2] H. L. Tierney, C. J. Murphy, A. D. Jewell, A. E. Baber, E. V. Iski, H. Y. Khodaverdian, A. F. McGuire, N. Klebanov, E. C. Sykes, *Nat. Nanotechnol.* **2011**, *6*, 625.
[3] H.-L. Lu, Y. Cao, J. Qi, A. Bakker, C. A. Strassert, X. Lin, K. H. Ernst, S. Du, H. Fuchs, H. J. Gao, *Nano Lett.* **2018**, *18*, 4704.
[4] J. K. Gimzewski, C. Joachim, R. R. Schlittler, V. Langlais, H. Tang, I. Johannsen, *Science* **1998**, *281*, 531.
[5] B. C. Stipe, M. A. Rezaei, W. Ho, *Science* **1998**, *279*, 1907.
[6] J. Michl, E. C. H. Sykes, *ACS Nano* **2009**, *3*, 1042.
[7] U. G. E. Perera, F. Ample, H. Kersell, Y. Zhang, G. Vives, J. Echeverria, M. Grisolia, G. Rapenne, C. Joachim, S. W. Hla, *Nat. Nanotechnol.* **2013**, *8*, 46.
[8] S. Jaekel, A. Richter, R. Lindner, R. Bechstein, C. Nacci, S. Hecht, A. Kühnle, L. Grill, *ACS Nano* **2018**, *12*, 1821.
[9] B.-Y. Choi, S. J. Kahng, S. Kim, H. Kim, H. W. Kim, Y. J. Song, J. Ihm, Y. Kuk, *Phys. Rev. Lett.* **2006**, *96*, 156106.
[10] V. Iancu, S.-W. Hla, *Proc. Natl. Acad. Sci. USA* **2006**, *103*, 13718.
[11] K. Scheil, T. G. Gopakumar, J. Bahrenburg, F. Temps, R. J. Maurer, K. Reuter, R. Berndt, *J. Phys. Chem. Lett.* **2016**, *7*, 2080.
[12] P. Liljeroth, J. Repp, G. Meyer, *Science* **2007**, *317*, 1203.
[13] S. Pan, Q. Fu, T. Huang, A. Zhao, B. Wang, Y. Luo, J. Yang, J. Hou, *Proc. Natl. Acad. Sci. USA* **2009**, *106*, 15259.
[14] W. Auwärter, K. Seufert, F. Bischoff, D. Ecija, S. Vijayaraghavan, S. Joshi, F. Klappenberger, N. Samudrala, J. V. Barth, *Nat. Nanotechnol.* **2012**, *7*, 41.
[15] T. Kumagai, F. Hanke, S. Gawinkowski, J. Sharp, K. Kotsis, J. Waluk, M. Persson, L. Grill, *Nat. Chem.* **2014**, *6*, 41.
[16] G. J. Simpson, S. W. Hogan, M. Caffio, C. J. Adams, H. Früchtl, T. van Mourik, R. Schaub, *Nano Lett.* **2014**, *14*, 634.
[17] J. N. Ladenthin, T. Frederiksen, M. Persson, J. C. Sharp, S. Gawinkowski, J. Waluk, T. Kumagai, *Nat. Chem.* **2016**, *8*, 935.
[18] J. Kügel, A. Sixta, M. Böhme, A. Krönlein, M. Bode, *ACS Nano* **2016**, *10*, 11058.
[19] J. A. Garrido Torres, G. J. Simpson, C. J. Adams, H. A. Früchtl, R. Schaub, *Nano Lett.* **2018**, *18*, 2950.
[20] J. Kügel, M. Leisegang, M. Bode, *ACS Nano* **2018**, *12*, 8733.
[21] R. Ohmann, L. Vitali, K. Kern, *Nano Lett.* **2010**, *10*, 2995.
[22] F. Mohn, J. Repp, L. Gross, G. Meyer, M. S. Dyer, M. Persson, *Phys. Rev. Lett.* **2010**, *105*, 266102.
[23] I. Swart, T. Sonnleitner, J. Repp, *Nano Lett.* **2011**, *11*, 1580.
[24] M. J. Comstock, N. Levy, A. Kirakosian, J. Cho, F. Lauterwasser, J. H. Harvey, D. A. Strubbe, J. M. Fréchet, D. Trauner, S. G. Louie, M. F. Crommie, *Phys. Rev. Lett.* **2007**, *99*, 038301.
[25] I. Franco, C. B. George, G. C. Solomon, G. C. Schatz, M. A. Ratner, *J. Am. Chem. Soc.* **2011**, *133*, 2242.
[26] L. Gerhard, K. Edelmann, J. Homberg, M. Valášek, S. G. Bahoosh, M. Lukas, F. Pauly, M. Mayor, W. Wulfhekel, *Nat. Commun.* **2017**, *8*, 14672.
[27] P. Erler, P. Schmitt, N. Barth, A. Irmler, S. Bouvron, T. Huhn, U. Groth, F. Pauly, L. Gragnaniello, M. Fonin, *Nano Lett.* **2015**, *15*, 4546.
[28] L. Gragnaniello, F. Paschke, P. Erler, P. Schmitt, N. Barth, S. Simon, H. Brune, S. Rusponi, M. Fonin, *Nano Lett.* **2017**, *17*, 7177.
[29] L. Vitali, G. Levita, R. Ohmann, A. Comisso, A. De Vita, K. Kern, *Nat. Mater.* **2010**, *9*, 320.
[30] I. Fernandez-Torrente, S. Monturet, K. J. Franke, J. Fraxedas, N. Lorente, J. I. Pascual, *Phys. Rev. Lett.* **2007**, *99*, 176103.
[31] P. Sessi, V. M. Silkin, I. A. Nechaev, T. Bathon, L. El-Kareh, E. V. Chulkov, P. M. Echenique, M. Bode, *Nat. Commun.* **2015**, *6*, 8691.
[32] R. D. Astumian, *Science* **1997**, *276*, 917.
[33] P. Reimann, P. Hänggi, *Appl. Phys. A* **2002**, *75*, 169.
[34] R. Ait-Haddou, W. Herzog, *Cell Biochem. Biophys.* **2003**, *38*, 191.
[35] L. Ji, Q. Fang, M. S. Yuan, Z. Q. Liu, Y. X. Shen, H. F. Chen, *Org. Lett.* **2010**, *12*, 5192.
[36] F. Furche, R. Ahlrichs, C. Hättig, W. Klopper, M. Sierka, F. Weigend, *WIREs Comput. Mol. Sci.* **2014**, *4*, 91.
[37] A. Schäfer, H. Horn, R. Ahlrichs, *J. Chem. Phys.* **1992**, *97*, 2571.
[38] J. P. Perdew, *Phys. Rev. B* **1986**, *33*, 8822.
[39] S. Grimme, *J. Comput. Chem.* **2004**, *25*, 1463.